minute. A sector which has been previously phased can be "trimmed" in 43 seconds. Tests were also performed to determine the resetting accuracy of the system. All phase-shifters were marked after being automatically set. The entire sector was randomly phased manually and then automatically rephased. The worst error measured was 3 degrees, with most phase-shifters returning to within 1 degree of their previous positions.

In addition to performing the essential function for which it was designed, the phasing system is beginning to be recognized as a very useful diagnostic tool. For instance, if the beam-induced pulse is observed as phasing proceeds down a sector, sudden decreases in the pulse amplitudes between adjacent test points immediately indicate loss of beam due to local mis-steering. Subdrive line and klystron-phase jitter and a variety of other malfunctions in the drive system can be easily recognized.

Acknowledgment

The authors are indebted to Dr. R. B. Neal and D. J. Goerz for their initial contributions in formulating the idea of beam-induction phasing, and to G. Jackson, Jr., J. R. Bordenave, P. V. Lee, and K. E. Holladay for their assistance in developing and testing the prototype system.

References

[1] R. Belbéoch and C. B. Williams, "Current variation detection technique of phasing linear electron accelerators," Stanford Linear Accelerator Center, Stanford University, Internal Memorandum, November 1962.
[2] W. J. Gallagher et al. (Drive and Phasing Committee), "Methods for phasing long linear accelerators," Stanford Linear Accelerator Center, Stanford University, Calif., Rept. M-101, November 1958.
[3] W. J. Gallagher et al. (Drive and Phasing Committee), "Methods of driving long linear accelerators," Stanford Linear Accelerator Center, Stanford University, Calif., Rept. M-102, December 1958.
[4] D. J. Goerz and R. B. Neal, "Phasing a linear accelerator from rf phase shift due to beam loading interaction," Stanford Linear Accelerator Center, Stanford University, Calif., Rept. M-103, December 1958.
[5] R. B. Neal et al. (Drive and Phasing Committee), "Comparison o methods of phasing long linear accelerators," Stanford Linear Accelerator Center, Stanford University, Calif., Rept. M-104, December 1958.
[6] R. B. Neal, "Transient beam loading in linear electron accelerators," Microwave Lab., Stanford University, Calif. Rept. ML-388, May 1957.
[7] G. A. Loew, "Non-synchronous beam loading in linear electron accelerators," Microwave Lab., Stanford University, Calif., Rept. ML-740, August 1960.

Stability and Gain Prediction of Microwave Tunnel-Diode Reflection Amplifiers

J. W. BANDLER

Abstract—**The Nyquist approach to stability is used in a form suitable for representation on a chart having conventional Smith chart scales. It is shown how the gain and stability of negative conductance reflection amplifiers of the tunnel-diode type can be *simultaneously* predicted on this chart. The technique described is particularly useful in the practical design of these amplifiers embedded in networks having complicated functions of frequency, as it involves predominantly graphical computations. A procedure is outlined for constructing immitance curves for the tunnel-diode, viewed either as a series or as a parallel circuit. An example of a 3-Gc/s amplifier operating in a rectangular waveguide is given.**

I. Introduction

A TUNNEL-DIODE, (Fig. 1), is potentially active at all frequencies from zero to resistive cutoff ω_R, above which it is regarded as passive. For low-noise figures and wide-band performance, amplification is restricted to around or less than a third of ω_R. Stability must, however, be considered over the whole active spectrum, and only when the effects of loading variations can be accounted for is it justifiable to concentrate on the desired amplification band.

Chapters VII–IX of Bode's book [1], especially the theorem on page 149, and the relevant parts of Henoch and Kvaerna's report [2] are useful in the following discussion. Also of interest are [3]–[6]. Poles P and zeros Z referred to in this paper are all contained in the r.h. p-plane. Real frequency loci are assumed to be plotted from just below $-\omega_R$ to just above $+\omega_R$. The tunnel-diode equivalent circuit parameters are considered, for simplicity, to be frequency independent.

Figure 2 shows the Nyquist plots of two typical tunnel-diodes. Figure 2(a) converts to Fig. 2(b) on adding sufficient series resistance, and vice versa on adding

Manuscript received March 11, 1965; revised May 4, 1965. The work reported in this paper was supported by the Science Research Council.

The author is with the Department of Electrical Engineering, Imperial College, London, England.

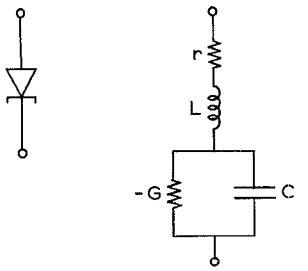

(a) (b)

Fig. 1. The tunnel-diode. (a) Symbolic. (b) Equivalent circuit.

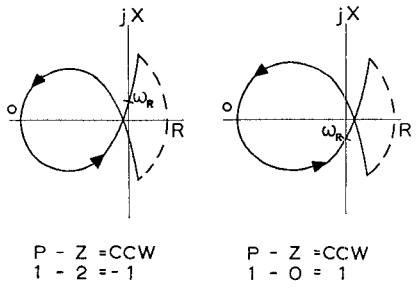

(a) (b)

Fig. 2. Tunnel-diode impedance characteristics $Z_D(j\omega)$. (a) $LG/C>r<1/G$, i.e., $\omega_R>\omega_X$. (b) $LG/C<r<1/G$, i.e., $\omega_R<\omega_X$.

sufficient series inductance [4]. Sometimes r and L are neglected, resulting in a parallel $-G$, C short-circuit (s.c.) stable equivalent circuit which can be stabilized by the addition of a positive G', where $G'>G$. A practical tunnel-diode is certainly not open-circuit (o.c.) stable, but it may or may not be s.c. stable according to whether its frequency characteristic is like Fig. 2(b) or Fig. 2(a), respectively.

II. Amplifier Gain Stability

Figure 3 represents the reflection amplifier considered here. Figure 4 shows the result of inverting the curves of Fig. 2. Note that poles invert to zeros and vice versa. $Y_1(p)$ is taken as pC_1, and for broadband performance, C_1 must be minimized [7]. The only three possible forms of $Y_D(j\omega)+Y_1(j\omega)$ are shown in Fig. 5. The curves of Fig. 5 invert to give Fig. 6. The Nyquist plot of $Z(j\omega)$ around a loop containing one tunnel-diode and one passive network in series must encircle the $Z(j\omega)$-plane origin once in a counterclockwise (CCW) direction [2], [3]. This is possible only if the plot starts in the l.h. $Z(j\omega)$-plane at dc.

Figure 7 shows two simple forms for $Z_2'(j\omega)$. The p-plane poles associated with Fig. 6 are carried through, and the resulting pole-zero arrangement associated with Fig. 7 is summarized in Fig. 8. Figure 6(c) has 3 r.h. p-plane poles associated with it, and it is not obvious what will happen to the frequency locus in the region in the l.h. $Z(j\omega)$-plane where the magnitude of the real component is greater than its dc value, the nature of the encirclements and hence stability being in some doubt. (In formulating Fig. 8, further encirclements above ω_R' are assumed nonexistent.) If

$$C_{1_{\text{total}}} < \frac{1}{\omega_R^2(L - Cr/G)} \tag{1}$$

where

$$\omega_R = \frac{G}{C}\sqrt{\frac{1}{Gr} - 1} > 0 \tag{2}$$

Fig. 6(a) results. If $r>LG/C$ [Fig. 2(b)], the aforementioned is inapplicable and Fig. 6(b) results. The remaining discussion considers the cases of Fig. 6(a) and Fig. 6(b) only.

For final stability, $Y_3(p)$ must ensure that $Y_3(p)+Y_2'(p)$ is free from zeros in the r.h. p-plane. [Figure 9 shows the resulting forms of $Y_2'(j\omega)$.] Since the poles of $Y_2'(p)$ are carried through, the stable admittance plot of the final network encircles the origin in a CCW manner as many times as $Y_2'(p)$ has poles in the r.h. p-plane. Examples in which a rectangular waveguide system defines $Y_3(j\omega)$ are given in Fig. 10.

For a reflection amplifier, the simplest configuration for Y_3 is Y_0+Y_3' (Fig. 3), where Y_0 represents a matched transmission-line, and Y_3' may describe a s.c. stub. The stability criterion for $\rho(p)$ is that r.h. p-plane poles be absent, in which case $|\rho(j\omega)|^2$ will represent the magnitude of the finite power gain of a stable amplifier.

Define $Y_L(j\omega)$ as

$$Y_L(j\omega) = -G_L + jB_L \tag{3}$$

where $-G_L$ and B_L are functions of ω. If $Y_0(\omega)$ is real

$$\rho(j\omega) = \frac{Y_0(\omega) + G_L - jB_L}{Y_0(\omega) - G_L + jB_L} \tag{4}$$

$|\rho(j\omega)|>1$ for reflection amplifiers, and it follows that the associated VSWR $s(\omega)$ is given by

$$s(\omega) = \frac{1 + |\rho(j\omega)|}{1 - |\rho(j\omega)|} \tag{5}$$

and is negative in this case [8]. If one extends the families of circles which make up the conventional Smith chart by including immittances with negative real parts, Fig. 11 is arrived at. This extension is quite impractical, apart from its availability. A simple transformation, however, brings the negative conductance (or resistance) plane into the conventional Smith chart as follows, and consequently facilitates its use with the minimum of alteration.

Define $Y_L'(j\omega)$ as

$$Y_L'(j\omega) = G_L' + jB_L' \tag{6}$$

then

$$\rho'(j\omega) = \frac{Y_0'(\omega) - G_L' - jB_L'}{Y_0'(\omega) + G_L' + jB_L'}. \tag{7}$$

Compare (4) and (7) such that

$$Y_0'(\omega) = Y_0(\omega); \qquad B_L' = B_L; \qquad G_L' = G_L$$

then

$$\rho'(j\omega) = \frac{1}{\rho^*(j\omega)} = \frac{\rho(j\omega)}{\rho^*(j\omega)\rho(j\omega)} = \frac{\rho(j\omega)}{|\rho(j\omega)|^2} \tag{8}$$

where $\rho^*(j\omega)$ is the complex conjugate of $\rho(j\omega)$. Vectors ρ' and ρ lie in the same line on the chart and rotate in the same sense when considered functions of position along the transmission-line. The center of the transformed chart corresponds to infinite gain, and constant ρ circles correspond to constant gain. The same chart is used to obtain a complete picture of the amplifier response, including regions when the conductance goes positive, bearing in mind the change in sign.

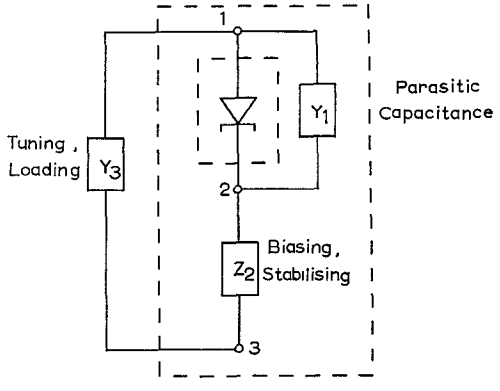

Fig. 3. Amplifier.

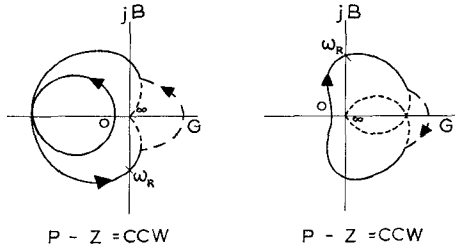

Fig. 4. Tunnel-diode admittance characteristics $Y_D(j\omega)$.

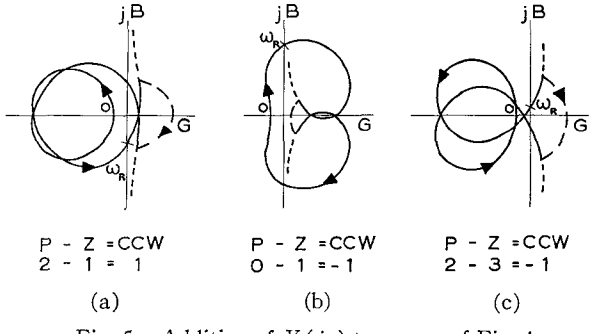

Fig. 5. Addition of $Y_1(j\omega)$ to curves of Fig. 4.

Let

$$Y_L(j\omega) = Y_2'(j\omega) + Y_3(j\omega) - Y_0(\omega). \tag{9}$$

Equation (9) tells us to consider the curves of Fig. 10 shifted to the left by $Y_0(\omega)$, and to consider stability in relation to $-Y_0(\omega)$ as a fixed set of real axis points, the encirclements of which are to be considered instead of the origin. Normalizing $Y_L(j\omega)$ to $Y_0(\omega)$, which may vary, the critical point becomes the fixed point $(-1, j0)$, i.e., the center of the previously derived Smith chart. CCW loci around the origin in the $Z(j\omega)$-plane or the $Y(j\omega)$-plane become CW loci in the chart about $(-1, j0)$, or vice versa, as explained by Fig. 12 which also

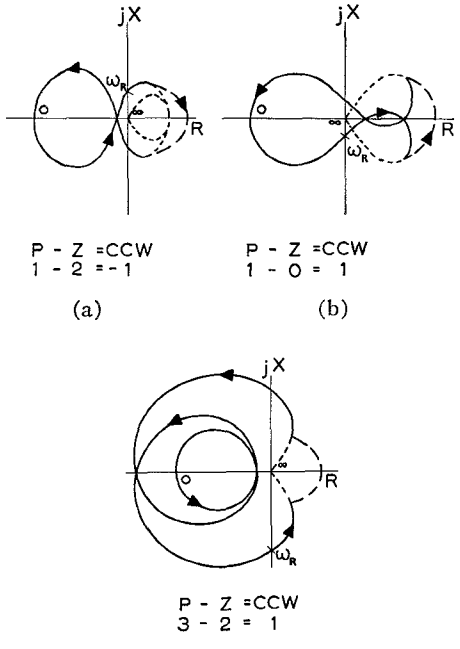

Fig. 6 Inversion of curves of Fig. 5 into the impedance plane.

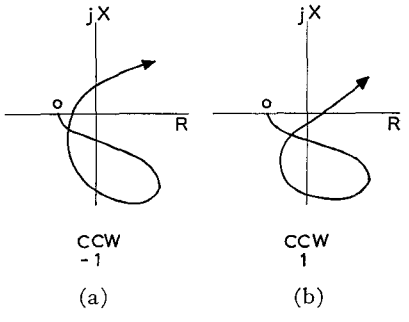

Fig. 7. Addition of $Z_2(j\omega)$ to curves of Fig. 6 to give $Z_2'(j\omega)$.

Fig.	Poles	Zeros Z	
	P	7(a)	7(b)
6(a)	1	2	0
6(b)	1	2	0
6(c)	3	4	2

Fig. 8. R.h. p-plane poles and zeros of $Z_2'(p)$.

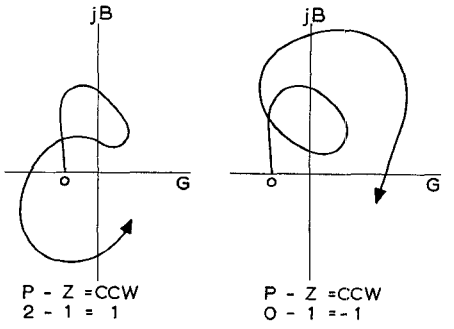

(a) (b)

Fig. 9. Inversion of curves of Fig. 7 to give $Y_2'(j\omega)$.

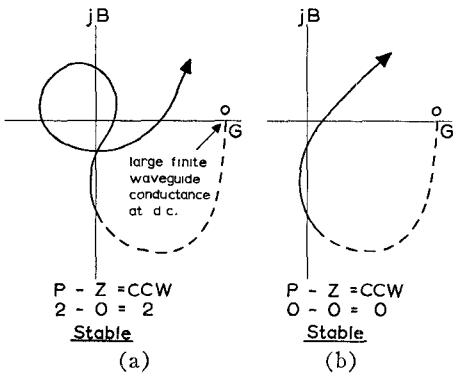

(a) (b)

Fig. 10. $Y_2'(j\omega)+Y_3(j\omega)$ when $Y_3(j\omega)$ is defined for a rectangular waveguide operating in the TE_{10}—mode under conditions shown in Fig. 14.

illustrates the consequences of the transformation of $\rho(j\omega)$. The stability criterion need be satisfied only on the new chart as it essentially accounts for the whole of the l.h. $Z(j\omega)$-plane or the l.h. $Y(j\omega)$-plane, plus the part of the r.h. plane from the imaginary axis of $Y_0(\omega) = G$. This has physical significance only when $Y_0(\omega)$ is actually present, as in the case of a matched line.

If ρ_C is the reflection coefficient of an imperfect circulator, and ρ is the reflection coefficient of the amplifier, then

$$1 - \rho(p)\cdot\rho_C(p) = 0 \tag{10}$$

must have no solutions in the r.h. p-plane [2], [3]. For $\rho(p)$ to represent inherently stable gain, it must have *no* r.h. p-plane poles, and since $\rho_C(p)$ represents a passive device, $1-\rho(p)\cdot\rho_C(p)$ has no r.h. p-plane poles, and, therefore, the plot of $1-\rho(j\omega)\cdot\rho_C(j\omega)$ must not encircle the origin of the $\rho(j\omega)$-plane, i.e., the center of the Smith chart $(1, j0)$, for stability. This can be rewritten as $\rho(j\omega)\cdot\rho_C(j\omega)$ must not encircle the point $+1$ which, assuming voltage reflection coefficients, is $(\infty, j\infty)$ for impedance coordinates or $(0, j0)$ for admittance coordinates. A new vector standing on the point $(1, j0)$ is obtained, whose rotation about the critical point is investigated. If

$$|\rho(j\omega)| \cdot |\rho_C(j\omega)| < 1 \tag{11}$$

the system is stable and independent of the relative phases of $\rho(j\omega)$ and $\rho_C(j\omega)$. Graphically represented, this requires that a plot of $\rho(j\omega)\cdot\rho_C(j\omega)$ be totally contained

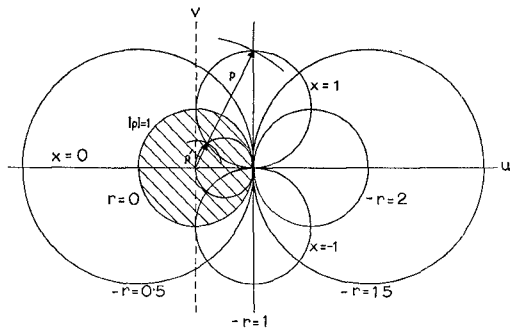

Fig. 11. Complete ρ-plane of which the conventional Smith chart forms a part (shaded area).

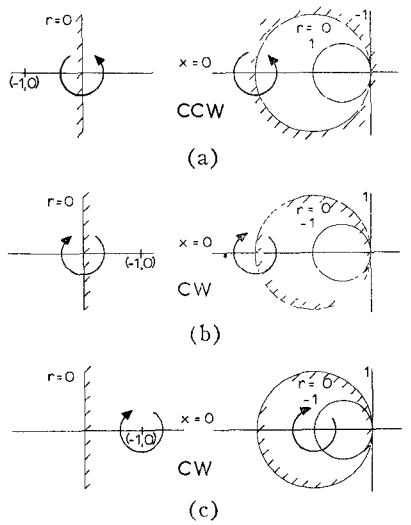

Fig. 12. Transformations and associated senses of rotation.

within the conventional Smith chart. This method does not, however, provide a "gain equation" whose stability and gain can simultaneously be predicted. If Y_C is the circulator admittance which is referred to the amplifier's terminals, then

$$\rho(j\omega) = \frac{Y_C^*(j\omega) - Y_L(j\omega)}{Y_C(j\omega) + Y_L(j\omega)} \tag{12}$$

gives the actual gain response. If all the admittances are normalized to $G_C(\omega)$, then $\rho(j\omega)$ is obtained from a Smith chart plot as previously suggested. The encirclements of $(-1, j0)$ in the analysis of stability are as previously explained.

III. Tunnel-Diode Chart

In this section, a very simple method of constructing tunnel-diode immittance characteristics is proposed using the Smith chart in the sense of a nomogram. The chart is first calibrated for the range of element values under consideration, so that this range is adequately displayed over the chart—C, L, $-R$, and $-G$ being set out along the center line, and X and B being set out around the imaginary axis (Fig. 13). The frequency scale is set out as follows.

If a straightedge is placed on the chart, then the product of the two numbers given by the points of

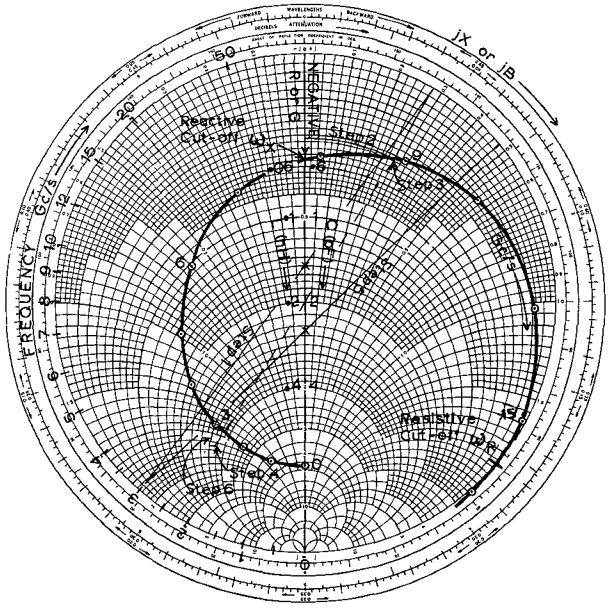

Fig. 13. Tunnel-diode chart normalized to 10 ohms or 100 mmhos.

INSTRUCTIONS

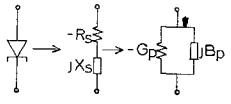

1) Locate f, C; find jB
2) Invert $-R$ to give $-G$
3) Add $-G+jB$
4) Invert to give $-R'+jX'$
5) Locate f, L; find jX
6) Add $r+jX$ to 4) to give $-R_S+jX_S$
7) Invert to give $-G_P+jB_P$
8) Invert $-G_P, jB_P$ to give $-R_P, jX_P$
9) Proceed. . . .

Example: $R=47$ ohms, $C=1.5$ pF, $r=0.75$ ohm, $L=0.25$ nH.

intersection of the straightedge with the outer (imaginary) axis will be found at the corresponding point of intersection of the straightedge with the center line (real) axis. Let the normalized scale on the chart read n. Assume that the B and C scales have been decided upon, and marked out. It is required to calculate

$$B = \omega C = 2\pi f C \tag{13}$$

when f and C are given. Then

$$knB = C \tag{14}$$

where k is a constant scale factor. Thus

$$kn = \frac{1}{\omega} = \frac{1}{2\pi f} \tag{15}$$

$$\therefore\ n = \frac{1}{2\pi f k}\,. \tag{16}$$

Choose convenient values of B and C, and obtain the corresponding n by a straightedge—hence k is known from (14). The frequency scale is then generated from (16) by inserting values for f and marking the n scale appropriately.

Referring to Fig. 13, let $B=100$ mΩ and $C=2$pF. Then $n=1.0$. From (14)

$$k = \frac{2}{1.0 \times 100} = \frac{1}{50}\ \text{second/rad/unit} \times 10^{-9}.$$

From (16), with f in Gc/s,

$$n = \frac{50}{2\pi f} = \frac{7.95}{f}\ \text{units}.$$

This whole process is repeated in a similar manner to calculate $X=\omega L$, but, with a certain amount of trial and error, all the scales can be adjusted so that they neatly fit in with each other. All the operations are carried out with a straightedge, a pair of dividers, and a pencil. The processes of inversion and addition, and so on, are the familiar ones.

IV. Example

A 3-Gc/s tunnel-diode reflection amplifier was constructed for S-band rectangular waveguide (Fig. 14). The diode was symmetrically mounted in a reduced height section for which the voltage-power definiton of Z_0 was assumed [9]. The variations with frequency of Z_0, which was 25 ohms at 3 Gc/s, were accounted for. The radial-line system [10], [11] presented zero impedance to the diode at 3 Gc/s. Variations in the coaxial-line's characteristic impedance, initially about 40 ohms, (adjustment of center rod diameter) and for the (vertical) width of the radial-line (by inserting or removing shims) were allowed for. Radiation from the end of the coaxial-line was assumed negligible [12]. An initial calculation showed that the diode's susceptance would be tuned out at 3 Gc/s by a stub length of 15 mm, leaving -35.4 ohms and resulting in a gain of 15 dB.

Although (1) is violated by the diode [case of Fig. 5(c) leading to Fig. 6(c)], it can be shown that the case of Fig. 6(a) can justifiably be assumed for the present purpose.

Figure 15 combines both the conventional and the negative resistance Smith charts; the behaviour of the locus is like that of Fig. 7(a). The relevant negative resistance portion is inverted into the admittance plane, and the tuning susceptance is added to give $Y_L(j\omega)$, leading to Fig. 16. From Figs. 10 and 12 it is known that stable operation results only when $Y_L(j\omega)$ encircles the critical point (namely, the center of the chart) twice in a CW direction, i.e., once in a CW direction for positive frequency only. Thus, only the continuous curves represent stable operation. The curves, plotted for particular values of l, are the predicted ones. Stable amplification was impossible for $l \leq 13$ mm, and oscillations were detected at the circulator output arm when the source was switched off.

Figures 16 and 17 show curves obtained by assuming an ideal band-rejection filter, i.e., that its impedance is identically zero in the frequency range of interest, corresponding to the maximum performance obtainable at 15 dB, limited mainly by the s.c. stub. Figure 17 shows the results of some attempts at approaching this performance by reducing the characteristic impedance of the coaxial-line and increasing the resistance per square of the terminating card.

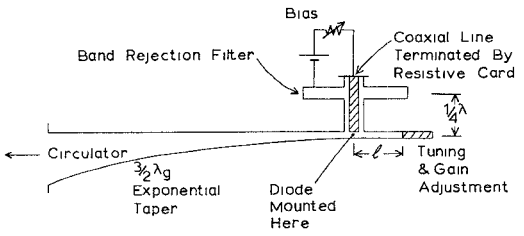

Fig. 14. Experimental amplifier.

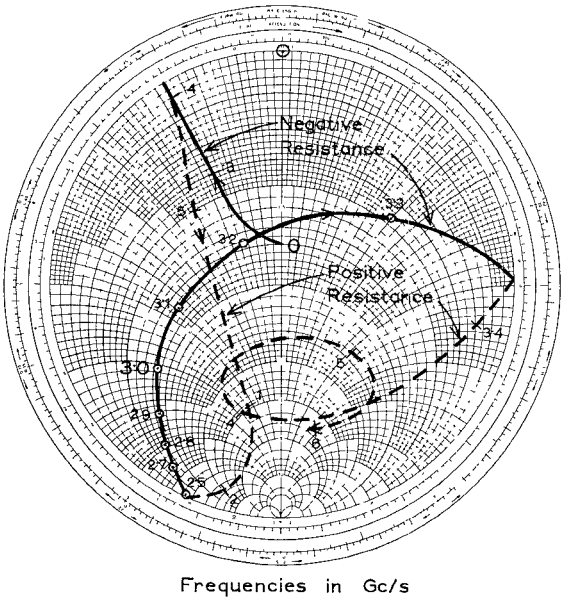

Fig. 15. Impedance between terminals 1 and 3 of Fig. 3, normalized to 10 ohms.

V. Conclusion

If Fig. 3 represents a tunnel-diode reflection amplifier, and if a matched transmission-line acting as both source and load forms part of Y_3, the gain and the stability of the arrangement can simultaneously be predicted by extracting the matched line, and plotting the remaining admittance (normalized) on a Smith chart (Fig. 16). Both the r.h. and the l.h. $Z(j\omega)$-plane or $Y(j\omega)$-plane are mapped into the Smith chart, CCW encirclements of the critical point, the center of the chart, in the former case remaining CCW, but becoming CW in the latter case (Fig. 12).

With reference to Fig. 16, it is noteworthy that unstable responses can resemble stable ones in every respect, except in the encirclement of the center of the chart.

Acknowledgment

The author thanks J. Roberts of the Electrical Engineering Department, Imperial College, who supervised this work. Many thanks are due to A. Wexler now with International Computers and Tabulators Ltd., London, for energetic encouragement and advice. The author is grateful to M. A. Lee of the Wembley Laboratories of Associated Semiconductor Manufacturers who provided the tunnel-diodes. M. Bandler, the author's father, is thanked for help in preparing the paper.

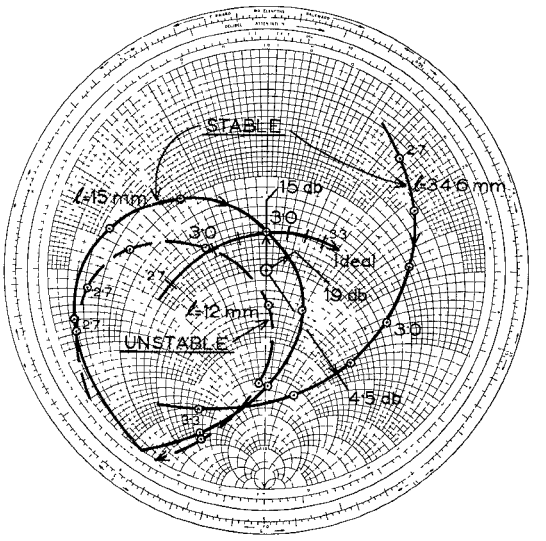

Fig. 16. Amplifier gain and stability, the rectangular waveguide's characteristic admittance, of the amplifier's admittance normalized to $Y_0(\omega)$, is given by encirclement in the center of the chart.

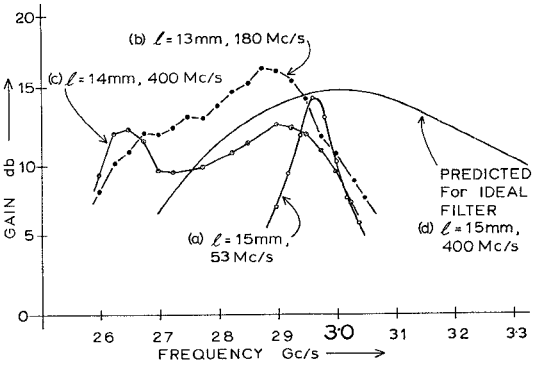

Fig. 17. Before and after attempts at broadbanding.

References

[1] H. W. Bode, *Network Analysis and Feedback Amplifier Design*. Princeton, N. J.: Van Nostrand, 1945.
[2] B. Henoch and Y. Kvaerna, "Broadband tunnel-diode amplifiers," Electron Devices Lab., Stanford University, Tech. Rept. 213-2, Astia Doc. AD 299 284, August 1962.
[3] B. Henoch and Y. Kvaerna, "Stability criteria for tunnel-diode amplifiers," *IRE Trans. on Microwave Theory and Techniques (Correspondence)*, vol. MTT-10, pp. 397–398, September 1962.
[4] U. S. Davidsohn, Y. C. Hwang, and G. B. Ober, "Designing with tunnel diodes, part 1," *Electronic Design*, vol. 8, pp. 50–55, February 3, 1960.
[5] G. L. Millican and L. F. Jelsma, "Radar electronics circuitry utilizing tunnel diodes," Apparatus Div., Texas Instruments Inc., Dallas, Tex., Final Rept. 5-46102-5, Astia Doc. AD 276 391, October 10, 1961.
[6] R. B. Whitson, "Impedance mapping in tunnel diode stability analysis," *IEEE Trans. on Circuit Theory (Correspondence)*, vol. CT-10, pp. 111–113, March 1963.
[7] W. J. Getsinger, "Prototypes for use in broadbanding reflection amplifiers," *IEEE Trans. on Microwave Theory and Techniques*, vol. MTT-11, pp. 486–497, November 1963.
[8] H. F. Lenzing and C. D. Elio, "Transmission line parameters with negative conductance loads and the 'Negative' Smith chart," *Proc. IEEE (Correspondence)*, vol 51, pp. 481–482, March 1963.
[9] B. C. DeLoach, "A new microwave measurement technique to characterize diodes and an 800-Gc cutoff frequency varactor at zero volts bias," *IEEE Trans. on Microwave Theory and Techniques*, vol. MTT-12, pp. 15–20, January 1964.
[10] S. Ramo and J. R. Whinnery, *Fields and Waves in Modern Radio*. New York: Wiley, 1953, pp. 395–401.
[11] B. C. DeLoach, Jr., "Radial line coaxial filters in the microwave region," *IEEE Trans. on Microwave Theory and Techniques*, vol. MTT-11, pp. 50–55, January 1963.
[12] R. F. Harrington, *Time-Harmonic Electromagnetic Fields*. New York: McGraw-Hill, 1961, pp. 110–113.